UNIVERSITY OF BREMEN
Faculty of Physics and Electrical Engineering
Institute of Environmental Physics

A sea ice concentration timeseries from 1991 - 2024 based on near 90 GHz microwave radiometer data

Adaption of the ASI algorithm to SSM/I and SSMIS data based on AMSR-2 data

Author: Isabel Krüll

Version: 1.0

April 30, 2026

Universität Bremen

iup

Contents

1 Introduction

There are several satellite sensors that have collected microwave emission data of the Arctic in the past decades, e.g., the SSM/I and SSMIS series, and the AMSR series. However, none of these sensors provides temporal coverage of several decades. Therefore, data from several sensors needs to be combined. The near 90 GHz channels of these sensors offer the highest spatial resolution and thus are attractive for regional studies and operational applications. The downside is a higher atmospheric sensitivity compared to higher frequencies. The idea is to create a consistent long-term sea ice concentration (SIC) time series from multiple passive microwave sensors. Key challenges are the slightly different operating frequencies of the sensors, temporal overlap and outlier in the datasets.
This document first gives an overview about the datasets. Then it introduces the outlier filters, and the tie point estimation method. It concludes with a description of the sensor adjustment procedure and the final SIC time series. The steps are as follows (Figure 2):

- Load brightness temperature data (NSIDC, EASE2 grid)
- Compute SIC, sea ice extent and sea ice area using the ARTIST Sea Ice (ASI) algorithm [Spreen et al., 2008]
- Apply outlier filters (Section 3)
- Estimate tie points from filtered SIC data via mean squared error (MSE) minimization (Section 4)
- Apply the calibration to all sensors using the selected tie point strategy (yearly median, see Section 5)
- Generate final time series (Section 6)

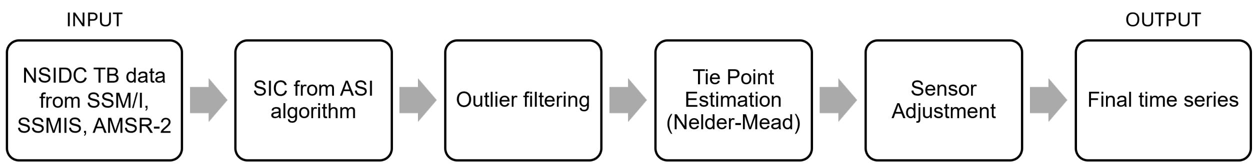

Figure 2. Processing pipeline for generating the final sea ice concentration time series from NSIDC brightness temperature data.

2 Datasets Overview

The primary input for the SIC time series algorithm consists of Level 2 gridded and resolution enhanced microwave brightness temperatures [Brodzik et al., 2016] from passive conically scanning radiometers [Remote Sensing Systems, 2022; NASA Earthdata, 2025]. The time series combines observations from three sensors: AMSR2, SSMIS, and SSM/I, providing continuous coverage from 1987 to the present. AMSR2, launched in 2012, provides 14 channels between 6.9 and 89 GHz at horizontal and vertical polarizations. SSMIS, onboard DMSP satellites (F16, F17, F18), offers 24 channels covering frequencies from 19 to 183 GHz. SSM/I, also flown on DMSP satellites (F08, F10, F11, F13, F14, and F15), provides seven channels between 19 and 85 GHz. Due to differences in native spatial resolution across channels and sensors, all observations are resampled to a common grid with a spatial resolution of 6.25 km using the Scatterometer Image Reconctruction (SIR) algorithm [Long et al., 1993]. For the SIC time series, only a subset of frequencies is used, namely channels centered around 18/19 GHz, 22/23 GHz, 36/37 GHz, and 85/89/91 GHz. Table 1 provides an overview of the selected frequencies and the temporal coverage of the three sensors. The data is mapped to EASE2 (Equal-Area Scalable Earth) grid and was processed by the National Snow and Ice Data Center (NSIDC) [Brodzik et al., 2016]. Figure 3 gives an overview of the available data from NSIDC. The data of F15 should not be used after July 2006 due to noisy retrievals [Hilburn and Wentz, 2008]. The SSMIS F18 was chosen for the testing of the time series adaption, however, it was not included in the final time series (Section 6) because SSMIS F16 provides a broader temporal coverage. Five satellite sensors were selected for the final time series based on temporal coverage and available data. Figure 4 provides an overview of these sensors and indicates the periods selected for the tie point estimation in Section 4.

Table 1. Satellite sensors and their respective operating frequencies [Remote Sensing Systems, 2022; NASA Earthdata, 2025].

Sensor	**Satellites**	**Sensor Frequencies**	**Temporal Coverage**
SSM/I	F08, F10, F11, F13	19, 22, 37, 85 GHz	1987 - 2008
SSMIS	F15, F16, F17, F18	19, 22, 37, 91 GHz	2000 - present
AMSR-2	GCOM-W1	18, 23, 36, 89 GHz	2012 - present

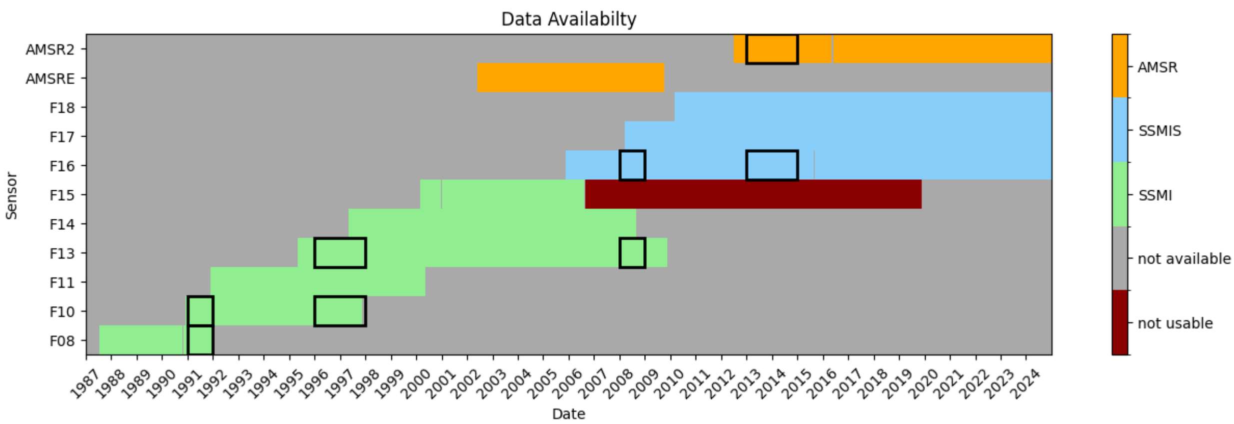

Figure 3. Overview of available data from NSIDC [Brodzik et al., 2016] for the sensors SSM/I, SSMIS and AMSR-2. The black rectangles indicate the selected overlap periods used to intercalibrate data between sensors (see Sections 4 and 5). The dataset spans 1987-2024. The data of F15 should not be used after July 2006 [Hilburn and Wentz, 2008].

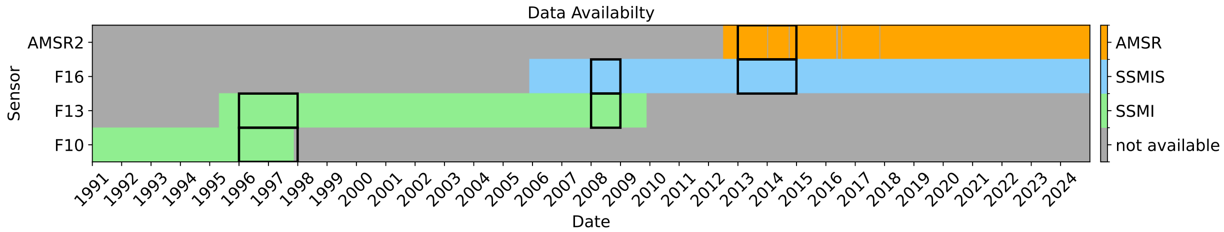

Figure 4. Overview of relevant SSM/I, SSMIS and AMSR-2 datasets. The black rectangles indicate the selected overlap periods used to intercalibrate data between sensors (see Sections 4 and 5). The dataset spans 1987-2024 and is provided by NSIDC [Brodzik et al., 2016].

3 Outlier Filtering

Before adjusting the different datasets to one another, the data is filtered in order to remove the outliers. Two different masks are applied, one is related to the number of *NANs* (Not-a-Number) for each day, and one is related to the daily change in sea ice extent. All dates where both masks are valid are excluded from the tie point optimization.

Filter 1
This filter excludes all dates where the number of NANs do not lie within ±15% of the yearly mean amount of NANs:

$$\#nan_{day} > \left((1 \pm 0.15) \cdot \frac{\sum_{n=1}^{365} \#nan_n}{365} \right). \tag{1}$$

Figure 5 demonstrates this filter using the SSMIS F18 sensor for the year 2013 as an example. It shows the daily sea ice extent in blue and the amounts of NANs per day in red. The yearly mean amount of NANs and the 15 % deviation from that is shown in gray. Apart from small deviations from the yearly mean nan count, there is one bigger outlier visible in mid April, which corresponds with the outlier in the sea ice extent.

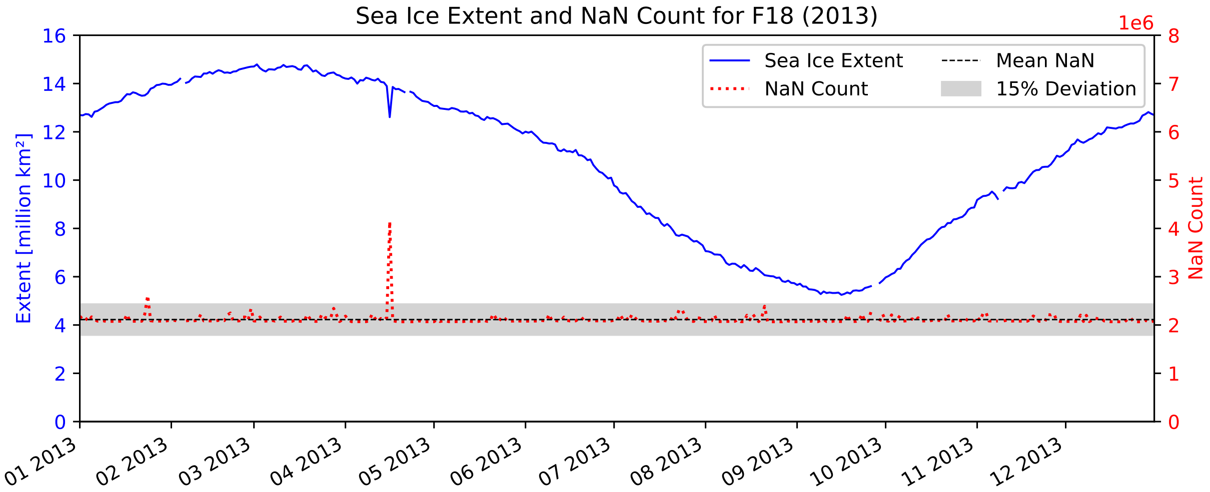

Figure 5. Sea ice extent data of SSMIS F18 in 2013 (blue). Daily amount of nan (red), yearly mean of nan count and the ±15% deviation from the mean (gray).

Filter 2

The second filter compares the change of sea ice extent from one day to another. It excludes all dates where the change in sea ice extent is bigger than ±0.25 million km^2:

$$|\mathrm{diff}(\mathrm{extent}_n, \mathrm{extent}_{n+1})| > 0.25 \cdot 10^6 \mathrm{km}^2. \tag{2}$$

The SSMIS F18 sensor is again used as an example to demonstrate the filter. Figure 6 shows the sea ice extent for 2013 in blue and the daily change in sea ice extent in green. The yearly mean in Δ sea ice extent and the $\pm$ 0.25 million km^2 deviation is shown in gray. The outlier in April is also visible in the Δ sea ice extent as strong change.

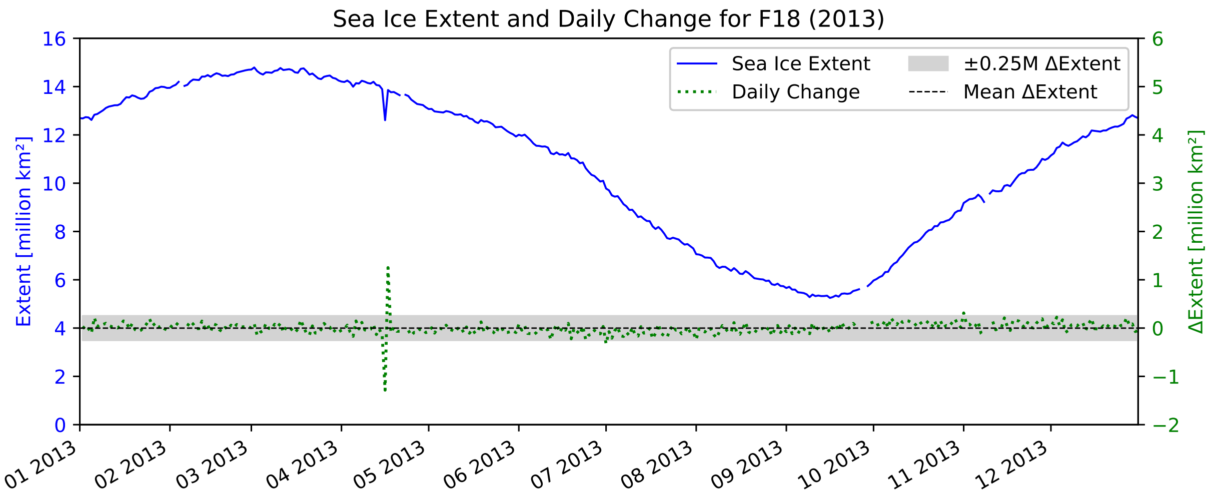

Figure 6. Sea ice extent data of SSMIS F18 in 2013 (blue). Daily change in sea ice extent (green), yearly mean of Δ sea ice extent and its $\pm$ 0.25 M km^2 deviation (gray).

Combining both filters results in the following mask for filtering out outliers:

$$\left[|\mathrm{diff}(\mathrm{extent}_n, \mathrm{extent}_{n+1})| > 0.25 \cdot 10^6 \mathrm{km}^2\right] \wedge \left[\#nan_{day} > \left((1 \pm 0.15) \cdot \frac{\sum_{n=1}^{365} \#nan_n}{365}\right)\right] \quad (3)$$

When the filter is applied, only the dates are kept where both filters are invalid. Figure 7 shows the resulting filtered sea ice extent together with the unfiltered extent as comparison.

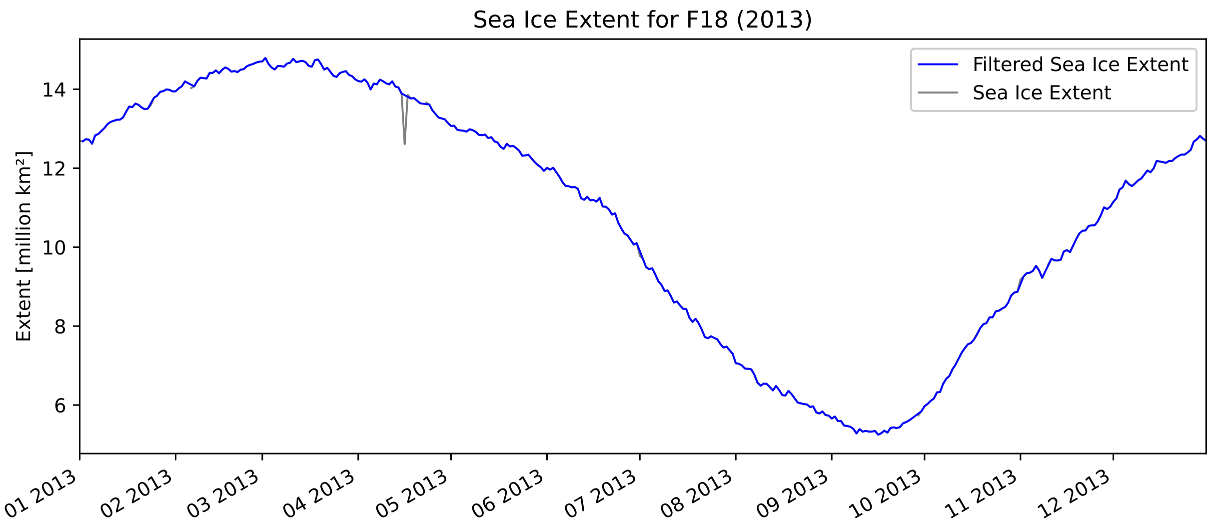

Figure 7. SSMIS F18: Comparison between unfiltered and filtered sea ice extent using the nan-count and Δ sea ice extent filter.

4 Tie Point Estimation

The sea ice concentration is computed from the brightness temperatures measured by the different microwave sensors using the ASI algorithm [Spreen et al., 2008]. The algorithm requires among other things two tie points as input, one for open water (P_0) and one for 100% sea ice concentration (P_1). The tie points depend on the operating frequencies of the sensors. Since the SSM/I and SSMIS sensors operate at other frequencies than the AMSR-2 sensor, they need to be adjusted to one another. The AMSR-2 data are used as reference and the other sensors are adjusted. The tie points for the SSM/I and SSMIS sensors are estimated by minimizing the mean squared error (MSE) between the sea ice concentration from AMSR-2 data and a SSMIS sensor:

$$min \left(\sum_{n=1}^{\#pixels} \left(SIC_{SSMIS} - SIC_{AMSR}\right)^2 \right). \quad (4)$$

For this multidimensional minimization, the Nelder-Mead-Algorithm is used [Nelder and Mead, 1965] by using the Python library *SciPy*. As starting point the tie points used for the AMSR-2 data are chosen: $P_0 = 47.0$, $P_1 = 11.7$.

5 Sensor Adjustment Procedure

For validating the tie point estimation with the Nelder-Mead-Algorithm, the method was first applied to only one sensor. Afterwards, it was extended to all SSM/I and SSMIS sensors.

Pilot Test

The SSMIS sensor F18 was chosen to test the tie point optimization for a three year period (2013 - 2015). First, the filters mentioned in Section 3 are applied to the two datasets to identify outliers and exclude these dates from the tie point estimation. Then, the optimum tie points for F18 for each date is computed. A 7-day rolling median is applied to reduce day-to-day noise while preserving seasonal trends. Figure 8 shows the optimized tie points for each day for the year 2013 together with the 7-day-rolling median and the yearly median. The yearly median results in $P_0 = 41.78$ and $P_1 = 10.74$, respectively, for the estimated tie points. While P_1 stays relatively constant throughout the year, P_0 shows stronger deviations from the yearly median, especially in summer. However, because the AMSR-2 ASI algorithm also uses constant tie points, we also use constant tie points without seasonal changes. This approach is also justified by the low variability of the more important P1 sea ice tie point. Further justification and evaluation of this choice are provided below.

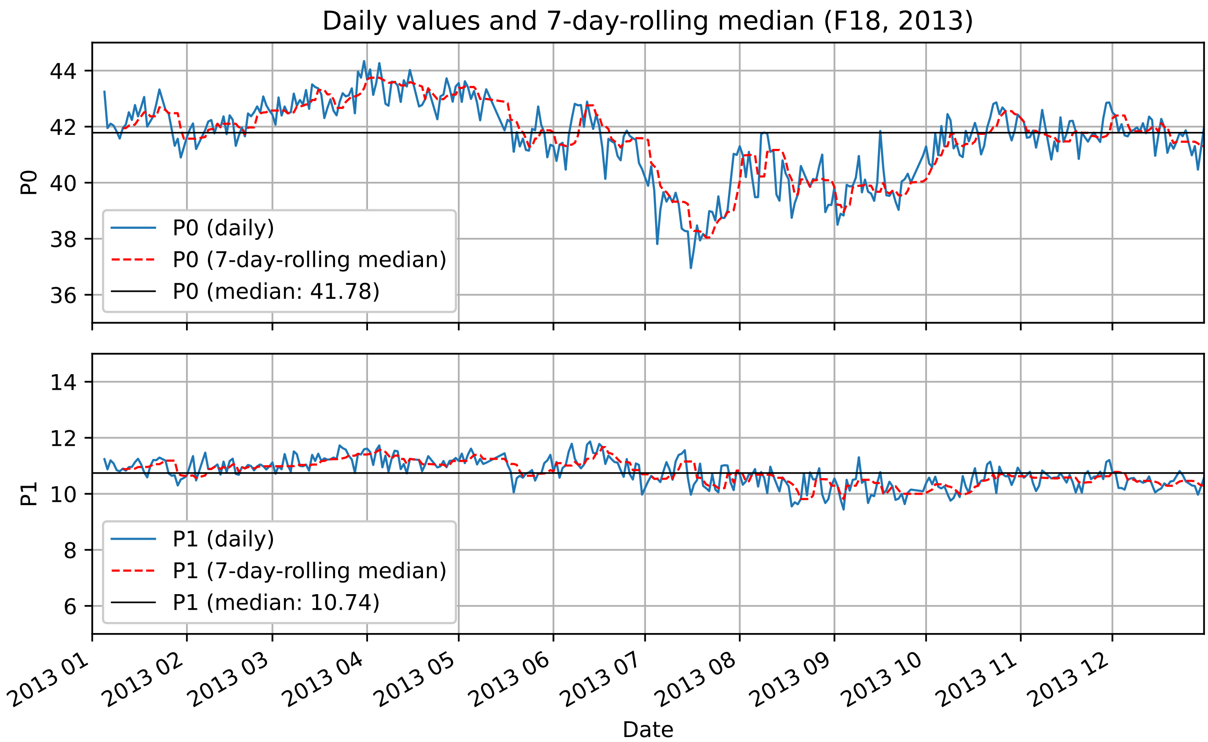

Figure 8. SSMIS F18: Optimized daily tie points for 2013, including their 7-day rolling median and yearly median. Results are shown for two tie points: open ocean (P0) and 100% sea ice concentration (P1).

The sea ice area can be computed from the sea ice concentration. Figure 9 shows the resulting sea ice area for F18 in 2013, computed from three different data: F18 data using the newly estimated tie points, F18 data using the AMSR-2 tie points and AMSR-2 data. The effect of the new tie points is clearly visible. The new F18 data resemble closely the data from AMSR-2. In the summer months, the stronger deviations in the daily tie points are visible as the plot of the new F18 data deviates slightly from the AMSR-2 data.

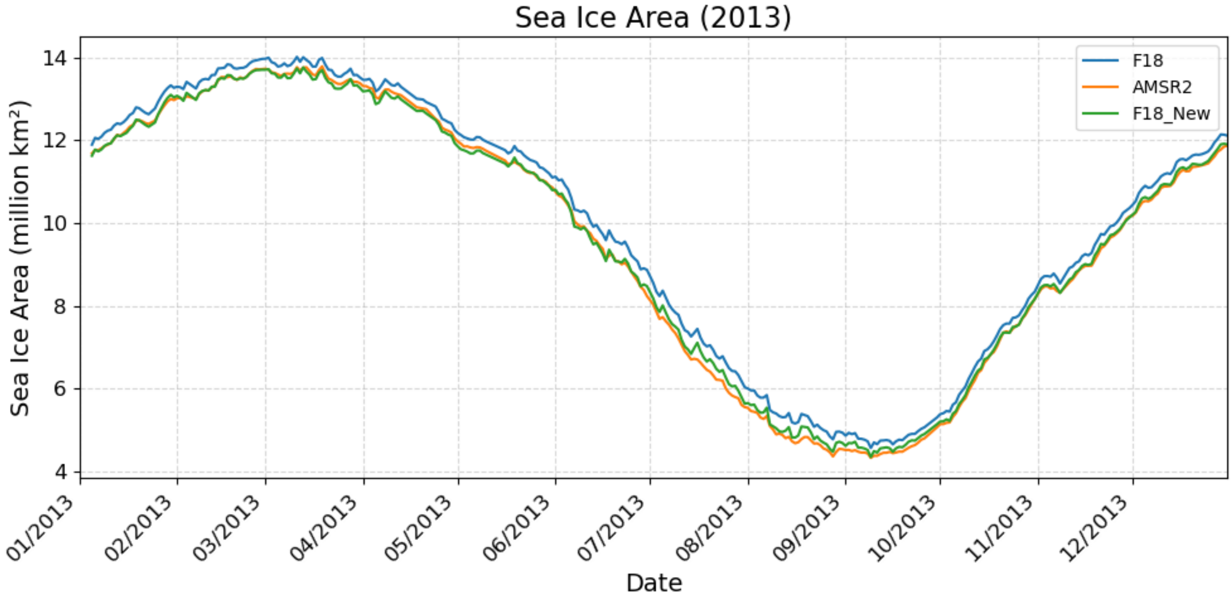

Figure 9. SSMIS F18: Comparison of sea ice area for 2013 derived using different approaches: AMSR2 data, SSMIS F18 data calibrated with AMSR2 tie points, and SSMIS F18 data calibrated with newly estimated tie points.

The pilot test (Fig. 9) has shown that the tie point estimation has worked. However, the question remains to what extent the varying tie points in the summer months influence the result and whether for the computation of the whole dataset tie points should be chosen on a daily basis or the same for the all the data from one sensor. Table 2 compares the daily tie points for some dates with the yearly median. As expected, P_1 is relatively consistent while P_0 varies more for all dates. Especially in summer (15.07.2013), the deviation of P_0 from the yearly median is strong with over 2.0. In order to assess whether the yearly median is still sufficient as tie point for the summer months, the resulting SIC maps from yearly and daily tie points are compared.

Table 2. SSMIS F18: Comparison of daily tie points with yearly mean values for selected dates (see Figure 8 for reference).

7-day rolling median	P_0	P_1
01.02.2013	41.6	10.6
01.04.2013	43.7	11.4
15.07.2013	39.2	11.2
01.12.2013	42.3	10.8
Yearly median	41.8	10.7

Figure 10 shows the SIC map for two dates and three different setups: one from AMSR-2 data, one from F18 with daily mean for tie points and one from F18 with the yearly median tie points. One date in summer (15.07.2013) and one date in winter (01.02.2013) is selected. As expected, the selected winter date shows only small differences between the setups. For the selected date in summer, the SIC map from daily and yearly tie points resemble one another, while they show larger differences to the SIC derived from AMSR-2 tie points. The difference maps in Figure 11 confirm this observation. The figure shows the difference in SIC between using AMSR-2 tie points and yearly tie points, and AMSR-2 tie points and daily tie points, respectively, for the same dates as in Figure 10. While the SIC map from the winter date shows only small differences, mainly visible at the ice edge, the other date shows bigger differences with deviations of more than 10 % SIC in some areas. However, these maps also show that these differences are similar for yearly and daily tie points. This leads to the assumption that these deviations are not due to the choice of tie points but caused by other factors. Since daily and yearly tie points produce similar results, yearly tie points are used.

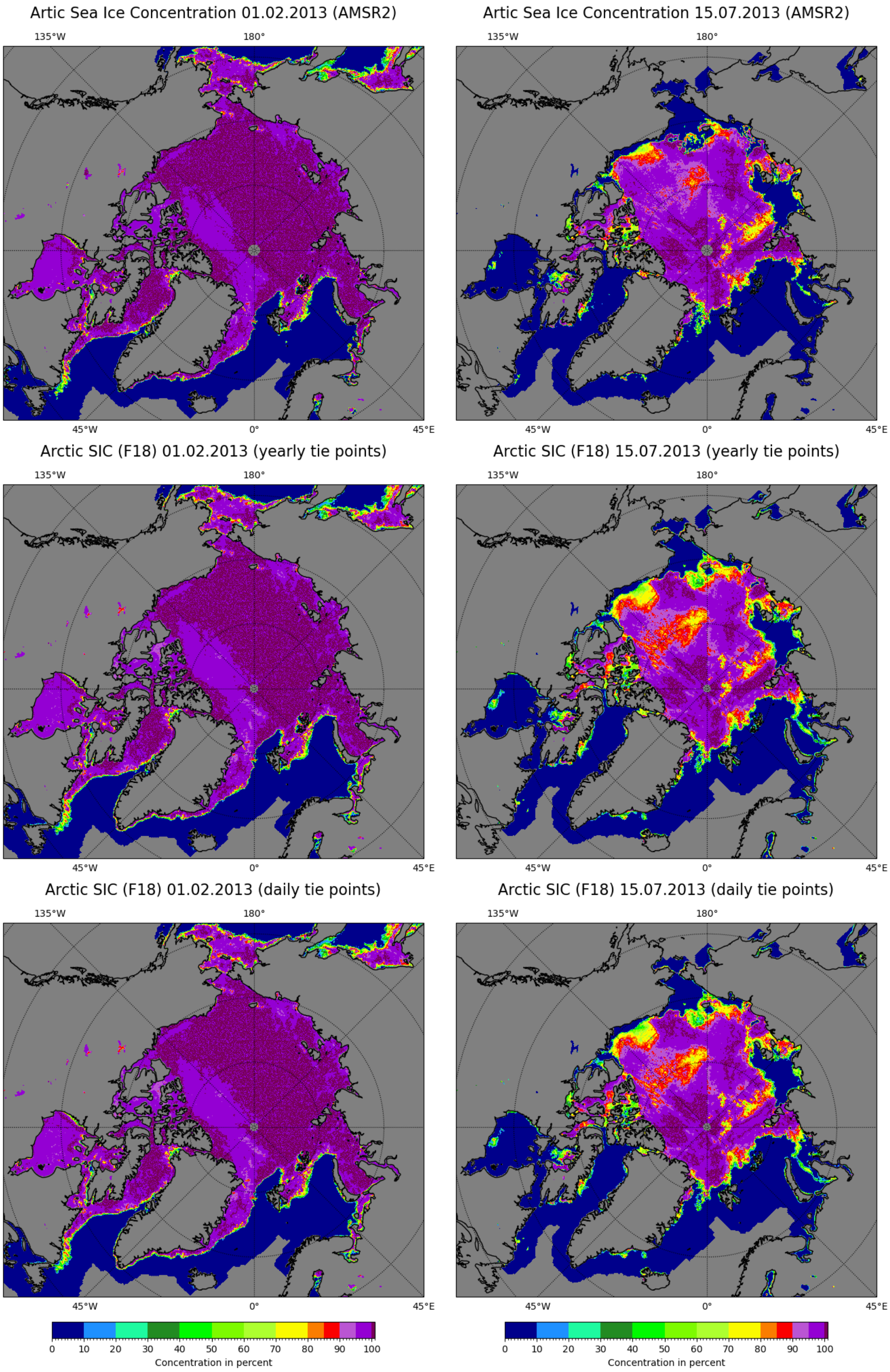

Figure 10. Comparison of sea ice concentration (SIC) maps derived from AMSR2 data, SSMIS data using yearly tie points, and SSMIS data using daily tie points. One date in winter date and one in summer are shown.

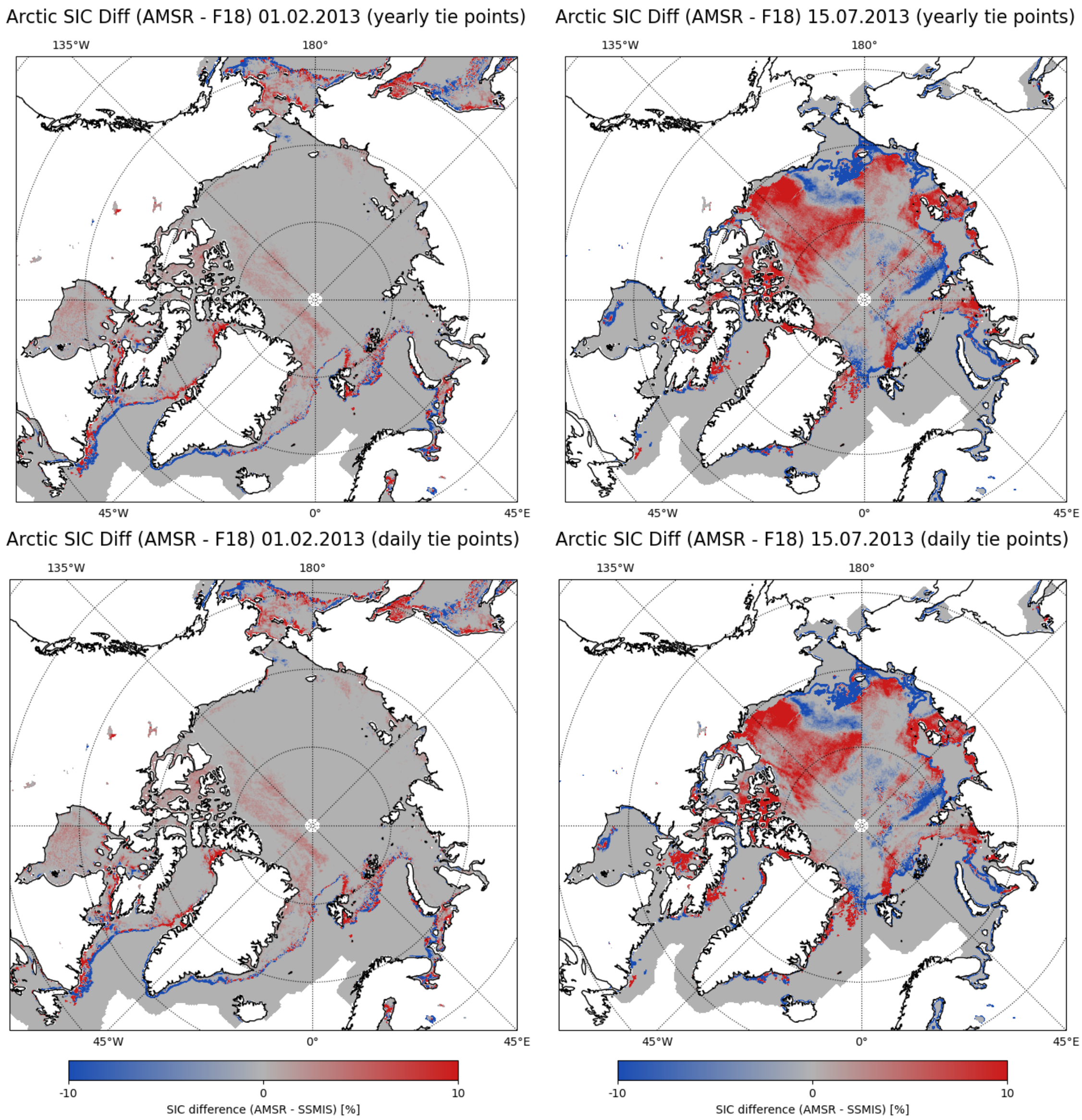

Figure 11. Difference maps between AMSR2- and SSMIS-derived sea ice concentration (Fig. 10) given in absolute percent SIC.

Expansion to three year period

The pilot test is extended to a three year period, using the same procedure as before for each year. Figure 12 shows the optimized tie points for the whole period and the 7-day-rolling median and the yearly median. Despite some outliers, the tie points show a yearly pattern with more variations in summer than in winter. Table 3 shows the yearly median and the 3-years median of the two tie points. The yearly median of the tie points is similar for all three years, or even the same in the case of P1. This leads to the conclusion that one year is already sufficient for the estimation of the tie points. However, for estimating the tie points of the remaining sensors, the longest overlapping period possible is chosen. Sometimes, this still results in an period of only one year due to incomplete datasets or small overlapping periods.

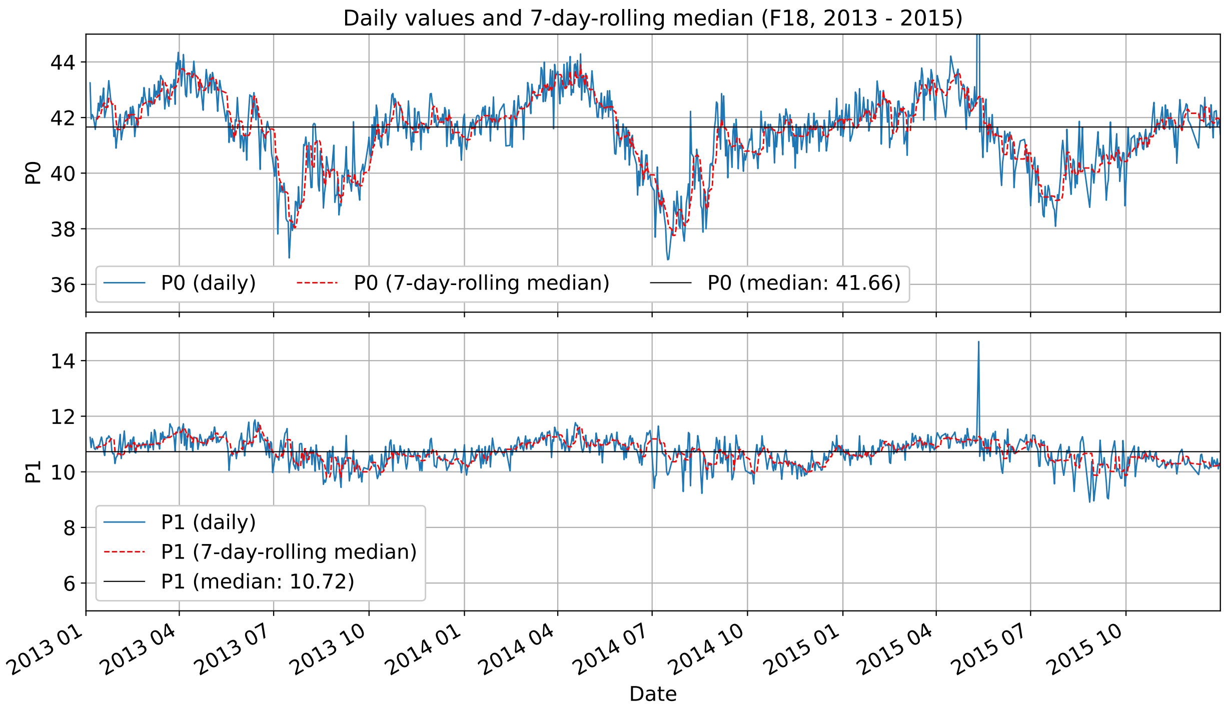

Figure 12. SSMIS F18: Optimized daily tie points from 2013 to 2015, including their 7-day rolling median and yearly median.

Table 3. SSMIS F18: Yearly median tie points and corresponding 3-year median values derived from the optimized daily tie points.

Median	P_0	P_1
2013 yearly median	41.8	10.7
2014 yearly median	41.6	10.7
2015 yearly median	41.6	10.7
3 years median	41.7	10.7

New Tie Points

Since the AMSR-2 sensor does not have an overlapping period with every SSM/I and SSMIS sensor, the sensors are adjusted subsequently, i.e., the optimum tie points for F16 are found by using AMSR-2 as reference, and the optimum tie points for F13 are found by using F16 as reference, and so on. Table 4 shows which sensors were chosen as reference for which tie point estimation and the reference period. It also shows the newly estimated tie points. They only differ slightly from one sensor to another.

Table 4. Overview of sensors and their newly estimated tie points, derived using the Nelder-Mead optimization algorithm.

Sensor	**(New) tie points**	**Reference period**	**Reference sensor**
AMSR-2	$P_0 = 47.0$, $P_1 = 11.7$	/	/
F18	$P_0 = 41.1$, $P_1 = 10.7$	2013 - 2015	AMSR-2
F16	$P_0 = 41.9$, $P_1 = 10.7$	2013, 2014	AMSR-2
F13	$P_0 = 41.4$, $P_1 = 10.7$	2008	F16
F10	$P_0 = 41.9$, $P_1 = 10.5$	1996, 1997	F13

6 Final Timeseries

For the final timeseries, the data from the most recent sensor available is always used (Table 4). The final timeseries product consists of daily sea ice concentration maps saved as *png-files* and their respective *nc-files*. Figure 13 shows the structure of the nc-file and the corresponding png-file of SSMIS F18 for February 1, 2012, as example. The nc-file contains the daily SIC values in EASE2 grid with a resolution of 6.25 km and the relevant gridding parameters. The png file shows the SIC map covering the whole Arctic down to the mid-latitudes (50° N). The daily sea ice area and sea ice extent values are saved in a *csv-file*. The sea ice area in square meters is defined as the total region covered by sea ice, and the sea ice extent in square meters is defined as the total region with at least 15 % sea ice cover. Figure 14 shows the resulting sea ice area time series from 1991 - 2024. As the difference between the data of two different sensors is low compared to the whole time series, the data is simply connected and not averaged in the overlapping period. The different colors of the plot indicate the different sensors used for the time series. There were still some outliers in the data. Therefore, the two filters described in Section 3 have been applied and the data points were connected to fill in the resulting data gaps.

```
<xarray.Dataset> Size: 33MB
Dimensions:  (time: 1, y: 2880, x: 2880)
Coordinates:
  * time     (time) datetime64[ns] 8B 2012-02-01
  * y        (y) float64 23kB 8.997e+06 8.991e+06 ... -8.991e+06 -8.997e+06
  * x        (x) float64 23kB -8.997e+06 -8.991e+06 ... 8.991e+06 8.997e+06
Data variables:
    SIC      (time, y, x) float32 33MB ...
    crs      float32 4B ...
Attributes:
    title:                   ASI Sea Ice Concentration
    summary:                 Daily ASI sea ice concentration for the Arctic
    info:                    Sea Ice Concentration data based on the ASI algo...
    author:                  Isabel Krüll (isakruel@uni-bremen.de)
    principal_investigator:  Gunnar Spreen (gunnar.spreen@uni-bremen.de)
    institution:             University of Bremen
    source:                  Satellite observation SSMIS F16
    Conventions:             CF-1.6
    date_created:            2026-04-16T13:04:24.584588
<xarray.DataArray 'crs' ()> Size: 4B
[1 values with dtype=float32]
Attributes:
    grid_mapping_name:              lambert_azimuthal_equal_area
    latitude_of_projection_origin:  90.0
    longitude_of_projection_origin: 0.0
    false_easting:                  0.0
    false_northing:                 0.0
    crs_wkt:                        PROJCRS["WGS 84 / NSIDC EASE-Grid 2.0 No...
```

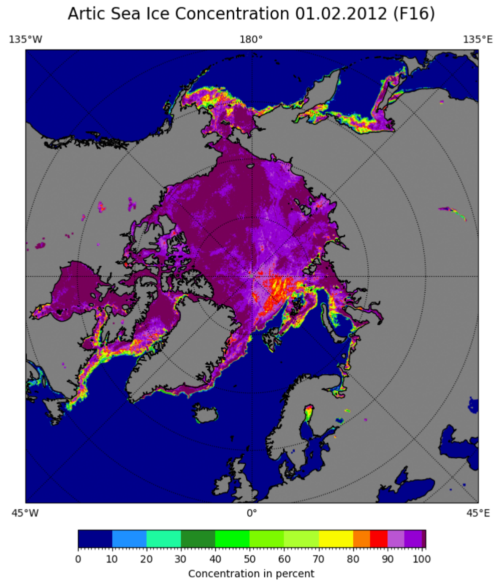

Figure 13. SSMIS F18: Example of the final nc- and png-file for February 1, 2012.

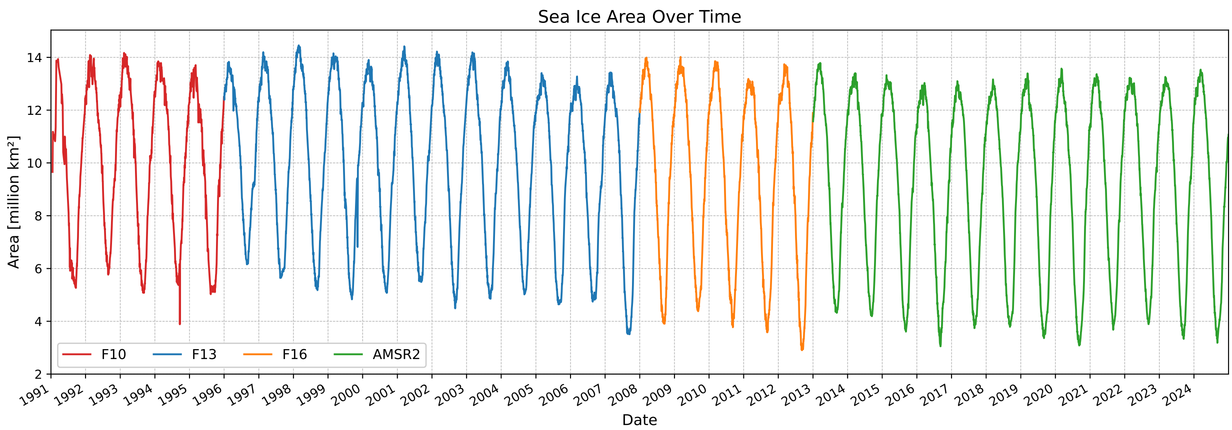

Figure 14. Final sea ice area time series derived from the calibrated dataset.

References

Mary Jo Brodzik, David Long, Molly Hardman, Aaron Paget, and Richard Armstrong. MEaSUREs Calibrated Enhanced-Resolution Passive Microwave Daily EASE- and ESDR-Grid 2.0 Brightness Temperature ESDR, Version 1, 2016. URL `http://nsidc.org/data/NSIDC-0630/versions/1`.

K. A. Hilburn and F. J. Wentz. Mitigating the impact of radcal beacon contamination on f15 ssm/i ocean retrievals. *Geophysical Research Letters*, 35(18), 2008. doi: https://doi.org/10.1029/2008GL034914. URL `https://agupubs.onlinelibrary.wiley.com/doi/abs/10.1029/2008GL034914`.

David G. Long, Philip J. Hardin, and Peter T. Whiting. Resolution enhancement of spaceborne scatterometer data. *IEEE Transactions on Geoscience and Remote Sensing*, 31(3): 700–715, 1993. doi: 10.1109/36.225519.

NASA Earthdata. Advanced Microwave Scanning Radiometer 2 (AMSR2). `https://www.earthdata.nasa.gov/data/instruments/amsr2`. Accessed: 2025-12-17, 2025.

John A. Nelder and Roger Mead. A Simplex Method for Function Minimization. *The Computer Journal*, 7(4):308–313, 1965. doi: 10.1093/comjnl/7.4.308.

Remote Sensing Systems. SSM/I and SSMIS Missions. `https://www.remss.com/missions/ssmi/`. Accessed: 2025-12-17, 2022.

G. Spreen, L. Kaleschke, and G. Heygster. Sea ice remote sensing using AMSR-E 89-GHz channels. *Journal of Geophysical Research: Oceans*, 113(C2), 2008. doi: https://doi.org/10.1029/2005JC003384. URL `https://agupubs.onlinelibrary.wiley.com/doi/abs/10.1029/2005JC003384`.